CHALMERS
FINITE ELEMENT CENTER

PREPRINT 2001–17

Eddy current computations using adaptive grids and edge elements

Y. Q. Liu, A. Bondeson, R. Bergström, C. Johnson,
M. G. Larson, and K. Samuelsson

Chalmers Finite Element Center
CHALMERS UNIVERSITY OF TECHNOLOGY
Göteborg Sweden 2001

CHALMERS FINITE ELEMENT CENTER

Preprint 2001–17

Eddy current computations using adaptive grids and edge elements

Y. Q. Liu, A. Bondeson, R. Bergström, C. Johnson,
M. G. Larson, and K. Samuelsson

CHALMERS

Chalmers Finite Element Center
Chalmers University of Technology
SE–412 96 Göteborg Sweden
Göteborg, September 2001

Eddy current computations using adaptive grids and edge elements
Y. Q. Liu, A. Bondeson, R. Bergström, C. Johnson,
M. G. Larson, and K. Samuelsson
NO 2001–17
ISSN 1404–4382

Chalmers Finite Element Center
Chalmers University of Technology
SE–412 96 Göteborg
Sweden
Telephone: +46 (0)31 772 1000
Fax: +46 (0)31 772 3595
www.phi.chalmers.se

Printed in Sweden
Chalmers University of Technology
Göteborg, Sweden 2001

EDDY CURRENT COMPUTATIONS USING ADAPTIVE GRIDS AND EDGE ELEMENTS

Y. Q. LIU, A. BONDESON, R. BERGSTRÖM, C. JOHNSON, M. G. LARSON, AND K. SAMUELSSON

Abstract. Results are presented from eddy current computations using adaptive techniques, based on rigorous *a posteriori* error estimates. The adaptivity restores the quadratic convergence with grid size of the magnetic energy, despite singularities occurring at corners. A new procedure is introduced to satisfy the solvability condition for the curl-curl equation. The methods are applied to a model of a hydrogenerator, with anisotropic conductivity and permeability. The ungauged formulation with both vector and scalar potentials gives very significant improvements in rate of convergence for this problem. Reasons for the improved convergence are discussed.

1. Introduction

Three-dimensional eddy current problems in realistic geometry are still demanding, and improvements in solution techniques are very valuable. In the present paper, we present results obtained using adaptive FEM techniques based on a recent *a posteriori* error estimate [1]. We also demonstrate and discuss the advantages of the "ungauged" formulation with vector and scalar potentials [2, 3, 4] which significantly improves the convergence rate for iterative solvers.

The methods are applied to a simplified model of a hydrogenerator, assuming a time-harmonic field. The geometry is shown in Fig. 1. The simulated region contains an angular segment of the four stacks at the axial end of the hydrogenerator. In the circumferential direction of the generator, the simulation region includes a slot and half a tooth, and its physical dimensions are 50 mm $\times$ 749 mm $\times$ 400 mm. The geometry is described in detail in [5]. The material properties are listed in Table 1. Both the electric conductivity and the magnetic permeability are anisotropic. The boundary conditions have been prescribed as vanishing normal magnetic flux density $B_n = 0$ on certain symmetry planes (essentially the surfaces facing the viewer in Fig. 1), and the tangential components of the magnetic field $\vec{H}$, as calculated from the Biot-Savart law for the currents in the rotor coil, on the remaining surfaces.

This work was supported in part by ABB Corporate Research and the Swedish Network for Applied Mathematics.

Y. Q. Liu and A. Bondeson are with the Department of Electromagnetics, Chalmers University of Technology, S-412 96 Göteborg, Sweden (e-mail {elfliu, elfab}@elmagn.chalmers.se)

R. Bergström, C. Johnson, M. G. Larson, and K. Samuelsson are with the Department of Mathematics, Chalmers University of Technology, S-412 96 Göteborg, Sweden (e-mail {ribe, claes, mgl, klassam}@math.chalmers.se) .

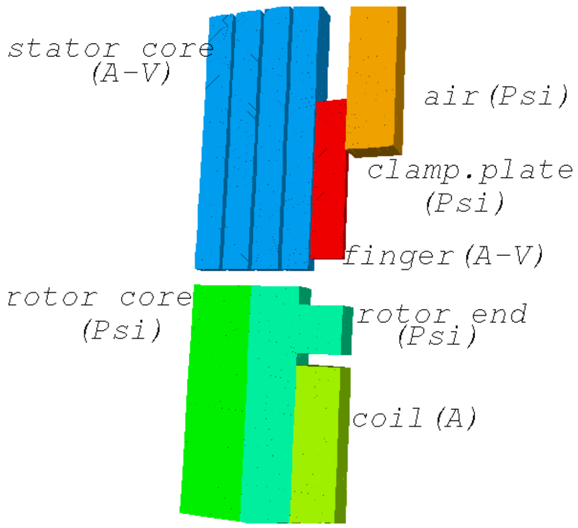

FIGURE 1. Geometry of the hydrogenerator model. The simulation region is half a tooth and a slot of the generator. The region is elongated in the radial direction of the generator (y) and narrow in the azimuthal direction (x).

	$\mu_{r,\perp\perp}$	$\mu_{r,zz}$	$\sigma_{\perp\perp}$[S/m]	σ_{zz} [S/m]
Stator core	465	13.9	2×10^6	0
Finger	3	3	1×10^7	1×10^7
Plate	600	600	0	0
Rotor end	600	600	0	0
Rotor core	3255	14.1	0	0

TABLE 1. Material parameters in different regions. $\perp$ refers to the xy-plane.

2. FORMULATION

In simply connected regions where the current density vanishes, we use the magnetic scalar potential ψ, such that $\vec{H} = \nabla\psi$, and solve $\nabla\cdot \bar{\bar{\mu}} \cdot\nabla\psi = 0$. The permeability $\bar{\bar{\mu}}$ is in general a tensor.

In coil regions, the current density is specified, and the magnetic vector potential satisfies

$$\nabla \times \mu^{-1}\nabla \times \vec{A} = \vec{J}_s \tag{1}$$

In conducting regions, the most efficient formulation uses both the vector and scalar potential, so that $\vec{E} = -j\omega\vec{A} - \nabla V$, and imposes no gauge [2, 3, 4]. Instead of a gauge condition, it is advantageous to impose the condition that the divergence of the conduction current vanish:

$$\nabla\times \bar{\bar{\mu}}^{-1} \nabla \times \vec{A} + \bar{\bar{\sigma}} \cdot (j\omega\vec{A} + \nabla V) = 0, \tag{2}$$

$$-c\nabla\cdot \bar{\bar{\sigma}} \cdot (j\omega\vec{A} + \nabla V) = 0. \tag{3}$$

We call this the AV formulation. c is a parameter that can be chosen. The conductivity $\bar{\bar{\sigma}}$ is typically a tensor to model laminations. We have solved (1) together with (2-3) using the lowest order edge elements for $\vec{A}$ and piecewise linear, nodal elements for V. The magnetic scalar potential ψ is also expanded in piecewise linear, nodal elements.

3. Solvability conditions

The $\nabla \times \mu^{-1}\nabla\times$ operator in (1) has a large nullspace, to which the source-term $\vec{J}_s$ must be orthogonal, in order for the equation to have a solution. Within the space of the lowest order edge elements, the nullspace for the discretized curl-curl operator consists of gradients of piecewise linear functions. Thus, the right-hand side of (1) must be orthogonal to the gradients of all piecewise linear functions $\bar{U}$. Although the exact coil currents are divergence-free, the orthogonality will in general not be exact for the finite element representation. To ensure $\nabla \cdot \vec{J}_s = 0$ numerically, we add a gradient as a correction to the prescribed current $\vec{J}$,

$$\vec{J}_s = \vec{J} - \nabla U. \tag{4}$$

We assume that (1) holds in a region Ω with the boundary conditions $\hat{n} \times \vec{A} = \hat{n} \times \vec{A}_t$ (to specify B_n) on $\partial\Omega_A$ and $\hat{n} \times \mu^{-1}\nabla \times \vec{A} = \hat{n} \times \vec{H}$ on $\partial\Omega_H$. U is determined by multiplying (1) by all gradients $\nabla\bar{U}$ of piecewise linears, and integrating over Ω:

$$\int_{\partial\Omega_H} \nabla\bar{U} \cdot (\hat{n} \times \vec{H}) dS = \int_\Omega \nabla\bar{U} \cdot (\vec{J} - \nabla U) dv \tag{5}$$

(U of course vanishes on all nodes on surfaces where $\vec{A}_t$ is specified.) Equations (4-5) remove any projection of $\vec{J}_s$ on the null space of the curl-curl equation and guarantee that (1) has a solution. Iterative solvers converge also for singular systems of equations if the right-hand side is consistent.

Another procedure to achieve consistency was given by Ren [6], who constructed a vector potential for the current. However, the new procedure is somewhat simpler, and, more importantly, includes the boundary conditions for $\vec{H}_t$. The left-hand side of (5) vanishes if $\vec{H} = \nabla\psi$ on the entire boundary of Ω.

Solvability has to be considered also in connection with the divergence condition (3). Since we do not want (3) to add any new information that is inconsistent with Ampère's law (2), the weak form of (3) is constructed by projecting (2) on test functions $\nabla\bar{V}$ that span the null space of the curl-curl operator, giving:

$$\int_{\partial\Omega_H} \nabla\bar{V} \cdot (\hat{n} \times \vec{H}) dS + \int_\Omega \nabla\bar{V} \cdot \bar{\bar{\sigma}} \cdot (j\omega\vec{A} + \nabla V) dv = 0 \tag{6}$$

4. Efficiency of iterative solvers

It has already been established for eddy current problems that iterative solvers converge much faster in the ungauged AV formulation (2-3) than in the pure A formulation or other gauged formulations [2, 3, 4]. Our study confirms this. In fact we find even larger improvement from the ungauged formulation than previous authors, presumably because the A formulation gives very badly conditioned matrices in the regions of anisotropic conductivity, as discussed in Sec 5

We have used the PETSc package for preconditioned Krylov methods [7]. For these eddy current problems, TFQMR (Transpose-Free Quasi-Minimized Residuals) is generally the most efficient solver. As preconditioner we used the ILU decomposition of a matrix obtained from the system matrix by multiplying the diagonal elements for $\vec{A}$ by a factor $\simeq 1.1$. Without such a multiplication, the preconditioning fails, apparently because of the null space of the curl-curl operator. The incomplete LU decomposition has been tried with different levels of fill in (ratio of the number of fill ins to the number of nonzero diagonal elements in the original matrix, indicated in parenthesis). Although the default ILU(1) works well for simple test problems, ILU(3) was considerably more efficient for the hydrogenerator problem. To reduce the memory requirement, we used ILU(2) for the largest grids, at the expense of a larger number of iterations.

Table 2 shows the number of iterations for the different grids, generated by adaptive mesh refinement, and different formulations in the conducting and non-conducting regions. In the coil region, we always use the A formulation in (1), with the source current modified according to (4-5).

Repr. ($\sigma \neq 0$, $\sigma = 0$)	Frequency	Number of unknowns (complex)	Iterations
(A,A)	0	16590	49
		26786	81
(A,A)	50Hz	16590	4622
		26786	6943
(AV,A)	50Hz	18336	269
		22640	327
		59134	453
(AV,ψ)	50Hz	12987	67
		27948	163
		67542	221

Table 2. Number of iterations for different formulations in the conducting and nonconducting regions for the static and time-harmonic hydrogenerator problem.

Notably, the number of iterations is very high for the A formulation at 50Hz. However, the AV-formulation achieves a very significant reduction in the number of iterations. The number of iterations is further reduced by using the magnetic scalar potential in the non-conducting regions.

5. Eigenvalue distribution

Insights into why the AV formulation speeds up the convergence can be gained by considering the eigenvalue distribution for the different formulations. When the discretization is free of "spurious solutions" (as are the discretizations using edge elements for the vector potential), it is sufficient to consider the eigenvalues of the analytic operators applied to complex exponentials $\exp(j\vec{k}\cdot\vec{r})$, where $\pi/|k|$ ranges from the longest spatial scale of the problem to the smallest, i.e., the grid size.

For isotropic σ and μ, the eigenvalues of the A formulation, where the operator is $\nabla\times\mu^{-1}\nabla\times + j\omega\sigma$, are $\lambda_{1,2} = k^2/\mu + j\omega\sigma$ (electromagnetic) and $\lambda_3 = j\omega\sigma$ (electrostatic $\vec{A} = \nabla\phi$).

For the AV operator in a homogeneous medium

$$\nabla\times\mu^{-1}\nabla\times\vec{A} + \bar{\bar{\sigma}}\cdot(j\omega A + \nabla V) = \lambda\vec{A} \tag{7}$$

$$-\nabla\cdot c\,\bar{\bar{\sigma}}\cdot(j\omega A + \nabla V) = \lambda V \tag{8}$$

the eigenvalues in the isotropic case are $\lambda_{1,2} = k^2/\mu + j\omega\sigma$ (electromagnetic), $\lambda_3 = c\sigma k^2 + j\omega\sigma$ (electrostatic) and $\lambda_4 = 0$ (gauge transformation). Thus, in addition to creating zero eigenvalues connected with gauge transformations, the AV formulation gives the electrostatic eigenvalues a real part. This brings them closer in the complex plane to the electromagnetic eigenmodes. Since all the non-zero eigenvalues have a part proportional to k^2, the AV formulation makes the problem elliptic (excepting the gauge transformations, of course). Since eigenvalues that are exactly zero do not affect iterative solvers if the right-hand side is consistent, and the non-zero spectrum for the AV formulation covers a smaller region of the complex plane, this formulation gives faster convergence. The gain from the AV formulation depends on the size of the imaginary part in comparison to the smallest and largest real parts, i.e., on the relation of the skin depth to the macroscopic scales and the grid size. Figures 2 and 3 show the eigenvalue distributionsfor a the test case of a discritized cube, for the A and AV formulations, respectively. Close examination shows that the separation between the electrostatic and electromagnetic eigenvalues of the matrix for the A formulation is not perfect (it would be if the normalization included the "mass matrix" $M_{ij} = \int \vec{N}_i\cdot\vec{N}_j dv$ where $\vec{N}$ denote the edge basis functions for the vector potential). However, when the number of elements is large enough to resolve the skin depth well, the eigenvalues separate as found analytically, and there is one "electrostatic" set very close to the imaginary axis.

For an anisotropic conductivity corresponding to laminations in the xy-plane, $\bar{\bar{\sigma}} = \sigma(\hat{x}\hat{x} + \hat{y}\hat{y})$, the differences are even more significant. For the A formulation the eigenvalues are: $\lambda_1 = k^2/\mu + j\omega\sigma$ (electromagnetic), while $\lambda_{2,3}$ (mixed electromagnetic/electrostatic) satisfy the quadratic equation

$$\lambda^2 - \lambda(k^2/\mu + j\omega\sigma) + j\omega\sigma k_\perp^2/\mu = 0 \tag{9}$$

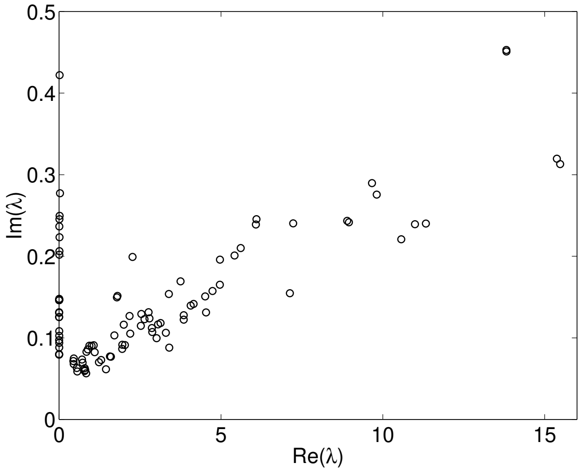

FIGURE 2. Numerical spectrum in the complex plane for a discritized conducting cube with the A formulation. The side of the cube is 1 m, the frequency 50 Hz, the conductivity 10^4 S/m, $c = 1/(\mu\sigma)$, and the number of edges is 250.

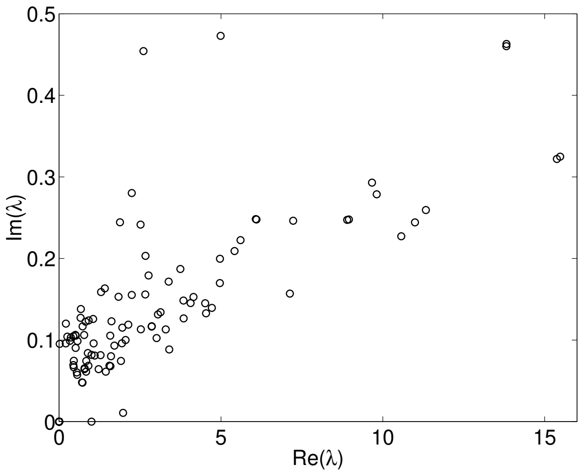

FIGURE 3. Numerical spectrum in the complex plane for a discritized conducting cube with the AV formulation. The parameters are the same as in Fig. 2.

with $k_\perp^2 = k_x^2 + k_y^2$. Equation (9) shows that numerically small eigenvalues occur (for nearly electrostatic modes) when $k_z^2 \gg k_\perp^2$

$$\lambda_3 \simeq j\omega\sigma k_\perp^2/k^2$$

Since the largest possible k is inversely proportional to the element size h, we see that the effective condition number (ratio of largest to smallest *non-zero* eigenvalue) of the A formulation, varies as h^{-4} to be compared with the h^{-2} scaling for the isotropic case. Thus, the A formulation gives an unfavorable scaling of the number of iterations when the grid is refined in the anisotropic case. This is confirmed by our numerical results.

For the AV formulation, the two mixed electromagnetic/electrostatic eigenvalues satisfy

$$\lambda^2 - \lambda(k^2/\mu + j\omega\sigma + k_\perp^2 c\sigma) + j\omega\sigma k_\perp^2/\mu + k_\perp^2 c\sigma k^2/\mu = 0 \tag{10}$$

[which reduces to (9) when $c = 0$]. These eigenvalues are well behaved when $k_z^2 \gg k_\perp^2$, in the sense that the small eigenvalues approach $k_\perp^2 c\sigma$, which is bounded from zero when the mesh is refined, and the condition number scales as h^{-2}. Thus, for laminated materials, the AV formulation strongly reduces the condition number in comparison with the A formulation.

6. Adaptivity

We have implemented a scheme for adaptive mesh refinement, based on an error estimate in energy norm [1]. Which elements are to be refined is decided from their contributions to the total error. For the AV-formulation, the contribution $I(e)$ from element e is:

$$\begin{aligned} I(e) = \sum_{f=1}^{4} \frac{h_f}{2} \left(\bar{\mu} |\delta \vec{H}_t|^2 + \frac{1}{\omega\bar{\sigma}} |\delta J_n|^2 \right) A_f \\ + h_e^2 \bar{\mu} |\vec{J}_s + \vec{J}_\sigma|^2 V_e \end{aligned} \tag{11}$$

where $\delta \vec{H}_t$ is the jump in tangential $\vec{H}$ across element boundaries, δJ_n the jump in the normal component of the conduction current, A_f the area of face f, V_e the volume of the element, and bars refer to averages defined in [1]. Similar estimates have been applied previously, on more heuristic grounds [8]. For the ψ formulation, we used the error indicator [9]

$$I(e) = \sum_{f=1}^{4} \frac{h_f}{2} \mu^{-1} |\delta B_n|^2 A_f.$$

Figure 4 shows that the energy $\int \vec{H} \cdot \vec{B} dv$ converges for the hydrogenerator problem as $O(h^2)$, where h is an average element size defined as $N^{-1/3}$, and N is the number of elements. Because of singular behavior at corners where the permeability is discontinuous, ($B \propto r^{-p}$, where r is the distance to the corner, and $p \simeq 1/3$ if μ has a large jump), computations with uniform grids only give $O(h^{4/3})$ convergence, so that adaptivity clearly improves the convergence. In addition to refining the grid at corners, the adaptivity also refines regions of the stacks where the skin effect makes the solution vary rapidly. Figure 5 illustrates how the magnetic field along a stator pole varies in the direction across the stacks. The skin effect is in clear evidence.

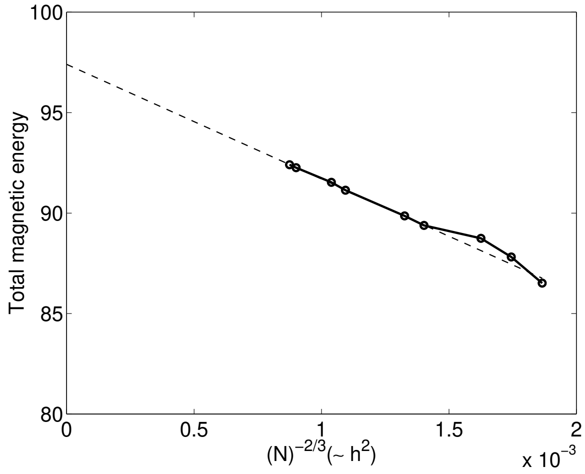

FIGURE 4. Convergence of the magnetic energy with adaptive grid for the hydrogenerator at 50 Hz.

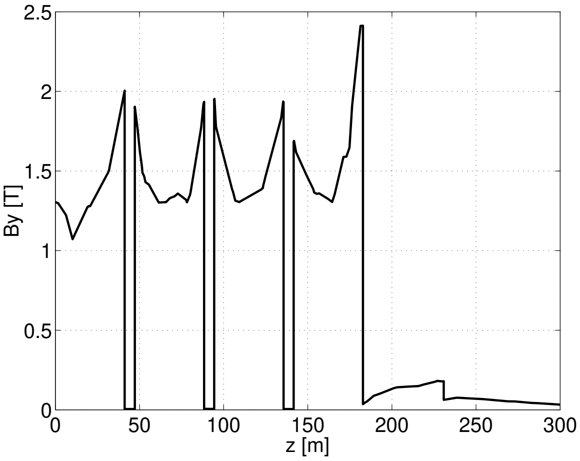

FIGURE 5. The radial component of the flux density along an axial line, crossing the stacks of the generator.

References

[1] R. Beck, R. Hiptmair, R. H. W. Hoppe, B. Wohlmuth, "Residual based a posteriori error estimates for eddy current computation", *ESAIM-Mathematical Modelling and Numerical Analysis*, vol. 34, pp. 159-182, January-February 2000.

[2] K. Fujiwara, T. Nakata, H. Ohashi, "Improvement of convergence of ICCG method for the A-ϕ method using edge elements", *IEEE Trans. Magn.*, vol. 32, no. 3, pp. 804-806, May 1996.

[3] R. Dyczij-Edlinger, O. Biro, "A joint vector and scalar potential formulation for driven high frequency problems using hybrid edge and nodal finite elements", *IEEE Trans. Microw. Tech.*, vol. 44, no. 1, pp. 15-22, January 1996.

[4] O. Biro, "Edge element formulations of eddy current problems", *Comput. Meth. Appl. Mech. Engrg.*, vol. 169, pp. 391-405, February 1999.

[5] M. Tuoma Holmberg, "Three-dimensional Finite Element Computation of Eddy Currents in Synchronous Machines", *PhD Thesis*, Tech. Rep. 350, Dept. Power Eng., Chalmers Univ. Tech., 1998.

[6] Zhuoxiang Ren, "Influence of the RHS on the convergence behavior of the curl-curl equation", *IEEE Trans. Magn.*, vol 32, pp. 655-658, May 1996.

[7] S. Balay, W. D. Gropp, L. McInnes, B. F. Smith, PETSc home page, http://www.mcs.anl.gov/petsc, 2000.

[8] S.Y. Hahn, C. Calmels, G. Meunier, J. L. Coulomb, "A posteriori error estimate for adaptive finite element mesh generation", *IEEE Trans. Magn.*, vol. 24, no. 1, pp. 315-317, January 1988.

[9] P. Fernandes, P. Girdinio, P. Molfino, M. Repetto, "A posteriori estimates for adaptive mesh refinement", *IEEE Trans. Magn.*, vol. 24, pp. 299-302, January 1988.

Chalmers Finite Element Center Preprints

2000–01 *Adaptive Finite Element Methods for the Unsteady Maxwell's Equations*
Johan Hoffman

2000–02 *A Multi-Adaptive ODE-Solver*
Anders Logg

2000–03 *Multi-Adaptive Error Control for ODEs*
Anders Logg

2000–04 *Dynamic Computational Subgrid Modeling* (Licentiate Thesis)
Johan Hoffman

2000–05 *Least-Squares Finite Element Methods for Electromagnetic Applications* (Licentiate Thesis)
Rickard Bergström

2000–06 *Discontinuous Galerkin Methods for Incompressible and Nearly Incompressible Elasticity by Nitsche's Method*
Peter Hansbo and Mats G. Larson

2000–07 *A Discountinuous Galerkin Method for the Plate Equation*
Peter Hansbo and Mats G. Larson

2000–08 *Conservation Properties for the Continuous and Discontinuous Galerkin Methods*
Mats G. Larson and A. Jonas Niklasson

2000–09 *Discontinuous Galerkin and the Crouzeix-Raviart element: Application to elasticity*
Peter Hansbo and Mats G. Larson

2000–10 *Pointwise A Posteriori Error Analysis for an Adaptive Penalty Finite Element Method for the Obstacle Problem*
Donald A. French, Stig Larson and Ricardo H. Nochetto

2000–11 *Global and Localised A Posteriori Error Analysis in the Maximum Norm for Finite Element Approximations of a Convection-Diffusion Problem*
Mats Boman

2000–12 *A Posteriori Error Analysis in the Maximum Norm for a Penalty Finite Element Method for the Time-Dependent Obstacle Problem*
Mats Boman

2000–13 *A Posteriori Error Analysis in the Maximum Norm for Finite Element Approximations of a Time-Dependent Convection-Diffusion Problem*
Mats Boman

2001–01 *A Simple Nonconforming Bilinear Element for the Elasticity Problem*
Peter Hansbo and Mats G. Larson

2001–02 *The $\mathcal{LL}^*$ Finite Element Method and Multigrid for the Magnetostatic Problem*
Rickard Bergström, Mats G. Larson, and Klas Samuelsson

2001–03 *The Fokker-Planck Operator as an Asymptotic Limit in Anisotropic Media*
Mohammad Asadzadeh

2001–04 *A Posteriori Error Estimation of Functionals in Elliptic Problems: Experiments*
Mats G. Larson and A. Jonas Niklasson

2001–05 *A Note on Energy Conservation for Hamiltonian Systems Using Continuous Time Finite Elements*
Peter Hansbo

2001–06 *Stationary Level Set Method for Modelling Sharp Interfaces in Groundwater Flow*
Nahidh Sharif and Nils-Erik Wiberg

2001–07 *Integration methods for the calculation of the magnetostatic field due to coils*
Marzia Fontana

2001–08 *Adaptive finite element computation of 3D magnetostatic problems in potential formulation*
Marzia Fontana

2001–09 *Multi-Adaptive Galerkin Methods for ODEs I: Theory & Algorithms*
Anders Logg

2001–10 *Multi-Adaptive Galerkin Methods for ODEs II: Applications*
Anders Logg

2001–11 *Energy norm a posteriori error estimation for discontinuous Galerkin methods*
Roland Becker, Peter Hansbo, and Mats G. Larson

2001–12 *Analysis of a family of discontinuous Galerkin methods for elliptic problems: the one dimensional case*
Mats G. Larson and A. Jonas Niklasson

2001–13 *Analysis of a nonsymmetric discontinuous Galerkin method for elliptic problems: stability and energy error estimates*
Mats G. Larson and A. Jonas Niklasson

2001–14 *A hybrid method for the wave equation*
Larisa Beilina, Klas Samuelsson, Krister Åhlander

2001–15 *A Finite Element Method for Domain Decomposition with Non-Matching Grids*
Roland Becker, Peter Hansbo and Rolf Stenberg

2001–16 *Application of stable FEM-FDTD hybrid to scattering problems*
Thomas Rylander and Anders Bondeson

2001–17 *Eddy current computations using adaptive grids and edge elements*
Y. Q. Liu, A. Bondeson, R. Bergström, C. Johnson, M. G. Larson, and K. Samuelsson

These preprints can be obtained from

`www.phi.chalmers.se/preprints`